



The Role of Load Control Modes in Determination of Mechanical Properties of Granite

Louis Ngai Yuen Wong^{1,2,3} · Fanzhen Meng^{1,4} · Tianyang Guo^{1,3} · Xiangchao Shi²

Received: 12 December 2018 / Accepted: 20 July 2019 / Published online: 3 August 2019
© Springer-Verlag GmbH Austria, part of Springer Nature 2019

Abstract

Circumferential strain-control tests were suggested to obtain the complete stress–strain curves (SSCs) of intact rock. However, compression test performed by the axial strain-control loading is mostly used to obtain the strength parameters and the SSCs. The influences of load control modes on the mechanical behavior of rock have not been fully investigated and understood. In this study, triaxial compression tests are conducted on granite specimens loaded by using both axial strain-control and circumferential strain-control modes to examine influences of load control modes on the determined mechanical properties. The occurrence mechanism and influencing factors of class II behavior are studied, and the potential application of the class II SSC in the evaluation of brittle failure of hard rock is also discussed. Results show that the peak strength, elastic modulus and fracture angle are generally higher in the axial strain-control test than in the circumferential strain-control test, and the failure in the former is also more violent than the latter under the same confining pressure. The much lower and constant circumferential deformation rate applied in the circumferential strain-control test is the dominant factor that favors the recovery of the complete post-peak SSC. The lower measured values of strength and elastic modulus are also associated with the lower deformation rate in the circumferential strain-control test, with a higher degree of damage and cohesion weakening occurring inside the rock. The development of the class II SSC is attributed to the axial strain recovery during the release of the stored elastic energy, which is influenced by the ratio of elastic energy to dissipated energy in the pre-peak stage, and is also associated with the consumed energy with respect to plastic deformation or initiation and propagation of new cracks in the post-peak stage. The class II SSC can aid the differentiation of the energy accumulation and consumption of different brittle rocks, which are usually characterized by a more abrupt and larger stress drop in the axial strain-control test. It can then be used to evaluate the strain rockburst potential of a particular rock type.

Keywords Load control modes · Strength · Failure mode · Post-peak behavior · Class II SSC

List of Symbols

SSC	Stress–strain curve
AE	Acoustic emission
σ_1	Maximum principal stress
σ_3	Minimum principal stress or confining pressure

$\sigma_1 - \sigma_3$	Differential stress
c	Cohesion
φ	Internal friction angle
α_f	Angle between the fracture plane and direction of σ_3
LVDT	Linear variable differential transducer

✉ Fanzhen Meng
mengfzh@hku.hk; xuilianmfzh@163.com

- ¹ Department of Earth Sciences, The University of Hong Kong, Pokfulam, Hong Kong, China
- ² State Key Lab of Oil and Gas Reservoir Geology and Exploitation, Southwest Petroleum University, Chengdu, China
- ³ The University of Hong Kong Shenzhen Institute of Research and Innovation, Shenzhen, China
- ⁴ College of Science, Qingdao University of Technology, Qingdao 266033, Shandong, China

1 Introduction

The compressive strength of rock, which is one of the most important parameters for the design and stability analysis of rock structure, is usually measured by using uniaxial and triaxial compression tests. The other parameters such as elastic modulus, internal friction angle and cohesion can be obtained from the stress–strain curve (SSC). Details of the testing methods for determining the uniaxial and triaxial

compressive strength and deformability of rock have been suggested by the International Society for Rock Mechanics and Rock Engineering (ISRM) (Bieniawski and Bernede 1979; Kovari et al. 1983). In these early suggested methods, the axial load is applied in a load control mode, and the stress will abruptly drop to a low value after overcoming the peak strength for the moderately and highly brittle rocks (Bieniawski and Bernede 1979). As such, the complete post-peak SSC cannot be properly obtained.

The complete SSC of an intact rock specimen has been recognized to be a useful indicator to interpret the rock failure process and to provide insight on in situ rock mass behavior, e.g., the extent of excavation-damaged zones, the proneness of rockburst and the brittle–ductile transition. Therefore, great effort has been made to experimentally obtain the complete SSC of rock specimen. Wawersik and Fairhurst (1970) obtained the complete SSCs of six different rock types by conducting post-peak cyclic loading and unloading uniaxial compression test. They classified the SSC as class I or class II, which corresponds to the negative or positive post-peak modulus, respectively. ISRM suggested detailed procedures to obtain the two types of SSCs (Fairhurst and Hudson 1999). Axial strain-control test is generally sufficient to obtain the complete SSC of specimens exhibiting class I behavior (soft and ductile rock). However, for moderately and highly brittle rock, the failure rupture occurs abruptly and explosively when the peak strength is reached under the axial strain-control mode. Therefore, circumferential strain has been suggested as a controlling variable to guide the application of the axial load for obtaining the complete SSC.

Since the pioneering work of Wawersik and Fairhurst (1970), different methods have been proposed to obtain the class II SSC. For example, the circumferential strain (Fairhurst and Hudson 1999), dilatant volumetric strain (Sano et al. 1982), a combination of load and displacement (Okubo and Nishimatsu 1985) and acoustic emission rate (Lockner et al. 1991) were separately suggested as the feedback signal to guide the axial stress application. Among the above listed methods, the circumferential strain-control is the most popular for testing brittle rocks (Fairhurst and Hudson 1999; Cai et al. 2010; Tarasov and Potvin 2013; Munoz et al. 2016a, b; Ai et al. 2016; Zheng et al. 2018), which was also the suggested method of ISRM to obtain the complete SSCs for rock specimens exhibiting brittle behavior.

The class II SSCs of different types of brittle rock obtained based on the aforementioned methods (circumferential strain, acoustic emission rate, etc., as the feedback signal of axial loading) have been applied in the following areas of research:

1. To study the crack nucleation and fault development of brittle rock at different stress levels especially in the post-peak stage (Tapponnier and Brace 1976; Wong 1982; Lockner et al. 1991; Lockner 1993; Nishiyama et al. 2002). The failure process is relatively more stable for the class II SSC as compared with the class I SSC, and the distribution and orientation of the mechanically induced cracks thus can be quantitatively analyzed in the post-peak stage.
2. To develop rock brittleness indices. The class II behavior of rock is regarded as a self-sustaining character (Tarasov and Potvin 2013), which is a manifestation of rock brittleness. Several brittleness indices based on the energy balance in the pre- or post-peak stages of class II SSCs have been proposed (Tarasov and Potvin 2013; Munoz et al. 2016a, b; Ai et al. 2016).
3. To evaluate the rockburst proneness of hard rock. A number of criteria have been developed to assess the rockburst potential by considering the energy accumulation and release calculated from the class II SSCs in the compression test (Cai et al. 2010; Wang et al. 2017).

Some studies have investigated the influences of axial loading rate (Okubo et al. 1990), rock type (Chen et al. 2010) and specimen geometry (Vogler and Stacey 2016) on the class II characteristics of rocks. Their findings suggested that anorthosite specimens with height-to-diameter ratios < 1 and sandstone specimens immersed in water for long time with low strength and elastic modulus exhibit class I behavior even though they were loaded under the circumferential strain-control mode. The theoretical and experimental analysis of Labuz and Biolzi (1991) also indicated that the class II behavior is a structural response rather than an intrinsic property of the material, which is associated with the size and geometry of the specimen.

The above listed studies contribute to the understanding of class II rock deformation behavior. The axial strain-control and circumferential strain-control tests have been suggested by the ISRM to obtain the complete class I and class II SSCs, respectively. However, compression test loaded under the axial strain-control is more commonly used to determine the strength parameters and the SSCs even for very hard rocks. In addition to the slower and more tedious procedures in the circumferential strain-control tests as compared with axial strain-control test, some other reasons also account for the less usage of circumferential strain-control tests to obtain the class II SSCs. The issues of how and why class II SSC occurs, what influences the class II behavior of rock, and how the class II SSC can be applied in practice are not fully understood. These discourage the widespread application of the class II SSCs. Although the load control mode has been recognized to impact the shape of the post-peak SSC, the influences of the two different load control modes on other key mechanical properties (strength, deformation,

failure modes, etc.) of rocks have been scarcely investigated. In view of the significant role of class II SSC in different aspects of rock engineering, there is a pressing need to comprehensively investigate the effects of different load control modes on the mechanical properties of rock, and to better understand the occurrence mechanism and influencing factors of class II SSC.

In this study, triaxial compression tests under different load control modes (axial strain-control and circumferential strain-control) are conducted on granite specimens. The deformation behavior, compressive strength, SSCs, failure modes and acoustic emission characteristics are studied and compared. The occurrence mechanism and influencing factors of class II SSCs are also particularly discussed.

2 Specimens, Experimental System and Method

2.1 Rock Specimen Preparation

In this study, the granite rock cores (diameter of 84 mm) are sampled from boreholes in the northwestern part of Hong Kong Island, from which standard cylindrical specimens ($\Phi 50 \times 100$ mm) are prepared according to the ISRM suggested method. Thin-section studies show that the granite is characterized by medium mineral grain size (with average grain of 0.92 mm), comprising 54% quartz, 23% K-feldspar, 14% plagioclase and 9% biotite.

2.2 Experimental Setup

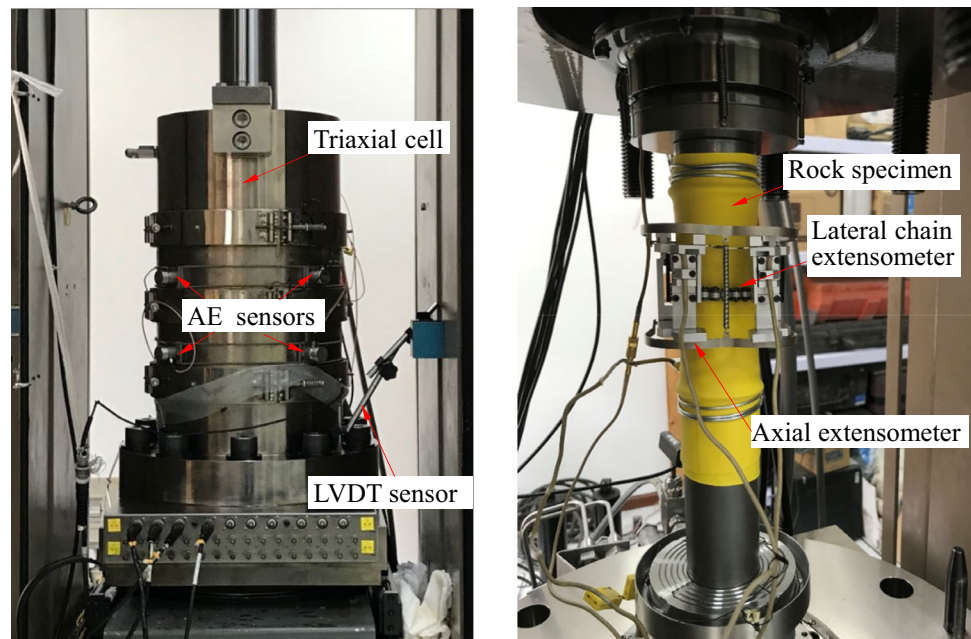
The test equipment consists of a MTS815 Flex Test GT rock test system and an acoustic emission (AE) monitoring system of PCI-II manufactured by the Physical Acoustic Corporation (PAC). The axial load and confining pressure capacity are 4600 kN and 140 MPa, respectively. The PCI-II AE system includes eight channels for the spatial AE-detection. The sampling rate is set to 1 million samples per second. The central frequency of AE sensors is 300 kHz. Because the AE sensors cannot withstand the high pressure, eight AE sensors are attached onto the exterior surface of the triaxial cell (four sensors for the upper end and lower end of the specimen, respectively, as shown in Fig. 1). The preamplifier gain is 40 dB, and the threshold is set to be 30 dB (Chen et al. 2015).

2.3 Test Scheme and Method

Considering that the failure process is violent for granite in the uniaxial compression test, and the highly fragile extensometer can be easily damaged due to the ejection of rock fragments, the lowest confining pressure is set to be 1 MPa to provide a small amount of lateral constraint in this study. Under high confining pressure, the failure process in the axial strain-control test is still extremely violent (very loud sound can be heard at the stress drop), so the confining pressure is capped at 40 to protect the extensometer from damage. The applied confining pressure is 1, 10, 20, 30 and 40 MPa in this study.

During the loading tests, the axial deformation of the rock specimen is measured by two axial extensometers attached

Fig. 1 MTS815 rock testing system



onto the specimen, a linear variable differential transducer (LVDT) mounted outside the triaxial cell, and the displacement of the platen (Fig. 1). The circumferential deformation is measured by a lateral chain extensometer (-2.5 to 8 mm) located at the specimen mid-height (Fig. 1). In the axial strain-control tests, the axial load is applied at a rate of 0.001 mm/s, while keeping the axial strain increasing monotonically. Similar to the method used by Fairhurst and Hudson (1999) to obtain the class II SSC, the axial load is first applied at an axial displacement rate of 0.001 mm/s. It is then adjusted to 0.04 mm/min (i.e., 0.00067 mm/s) under circumferential strain-control when the differential stress reaches approximately 50% of the peak strength (the peak strength is estimated from the experimental results in the axial strain-control tests under the same confining pressure conducted prior to the circumferential strain-control test).

3 Results and Analysis

3.1 Comparison of the Axial Strain Measured by the Three Methods

Figure 2 shows the SSCs of the granite under confining pressure of 1 and 30 MPa, respectively, in the axial strain-control load test. The axial strain of the specimen is calculated from the measurements of the axial extensometers (the left green and red curves), LVDT (the middle black curve) and the platen displacement (the right blue curve). The two cases clearly show that the axial strain measured by extensometers is much smaller than that measured by external LVDT and the platen displacement. Besides, the axial strain measured from the platen displacement is a little larger than that from the LVDT sensor, both of which have very similar variation

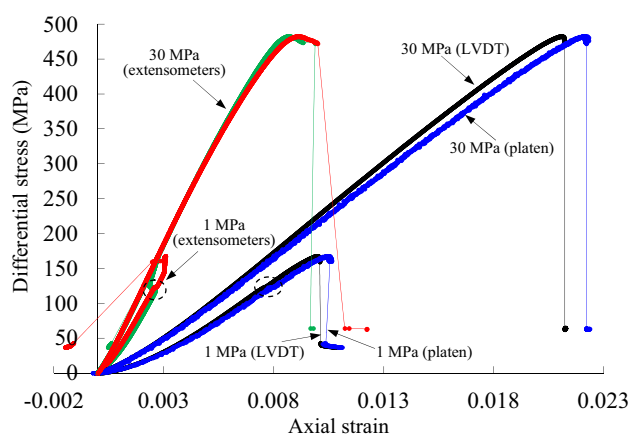


Fig. 2 Comparison of the stress–axial strain curves from axial extensometers (green and red curves), LVDT (black curve) and platen displacement (blue curve) for granite under 1 and 30 MPa confining pressure in the axial strain-control loading test (colour figure online)

trend. These findings are consistent with Munoz et al. (2016b) who measured the axial deformation of sandstone specimen in the uniaxial compression test by axial strain gauges, LVDT, platen displacement and 3D digital image correlation.

The strain measurement from LVDT and platen displacement includes the rock deformation, bedding error and machine compliance (Munoz et al. 2016b). In contrast, the axial extensometers or strain gauges which are attached on the surface of the rock specimen measure the true deformation of rock under loading. However, the measured strain values are dependent on the range that the extensometer covers or the length of the strain gauges. Only when the gauges or extensometer covers the whole length of the specimen can the axial deformation of the rock specimen be accurately obtained.

Figure 2 also indicates that the two strains obtained from the extensometers are not completely consistent. A small stress fluctuation occurs when the differential stress reaches 122 MPa under 1 MPa confining pressure (as indicated by the circle in Fig. 2), after which the axial strain from the extensometer starts to deviate from each other. This kind of leap and irregular characteristics of the axial strain from extensometers are very common in our tests, especially around or after peak strength, which we consider is attributed to the local fracture on the surface of rock specimen near or after peak strength. The extensometer data will be influenced or even become invalid if fractures occur in the coverage of the extensometers. In view of this, we adopt the axial strain measured from the LVDT to plot the SSCs in this study for a better comparison.

3.2 SSCs

The SSCs and dilation curves of granite under different confining pressures loaded by axial and circumferential strain-control modes are shown in Figs. 3 and 4. In Fig. 3a, the granite shows very strong elastic–brittle characteristics when loaded by the axial strain-control. The differential stress increases almost linearly to the peak strength, and then decreases abruptly to a residual value for all the confining pressures. A very loud sound can be heard associated with the stress drop. The concave upward shape of the stress curves in the early stage is very likely to be due to the compaction of rock specimen and the adjustment of the contact between rock and platens.

Figure 4a shows the SSCs for granite when loaded by circumferential strain-control, which behaves differently from those loaded by axial strain-control, especially in the post-peak stage. Similar to the axial strain-control tests, the differential stress increases almost linearly with increasing axial strain before the peak strength. However, both the differential stress and axial strain decrease beyond the peak

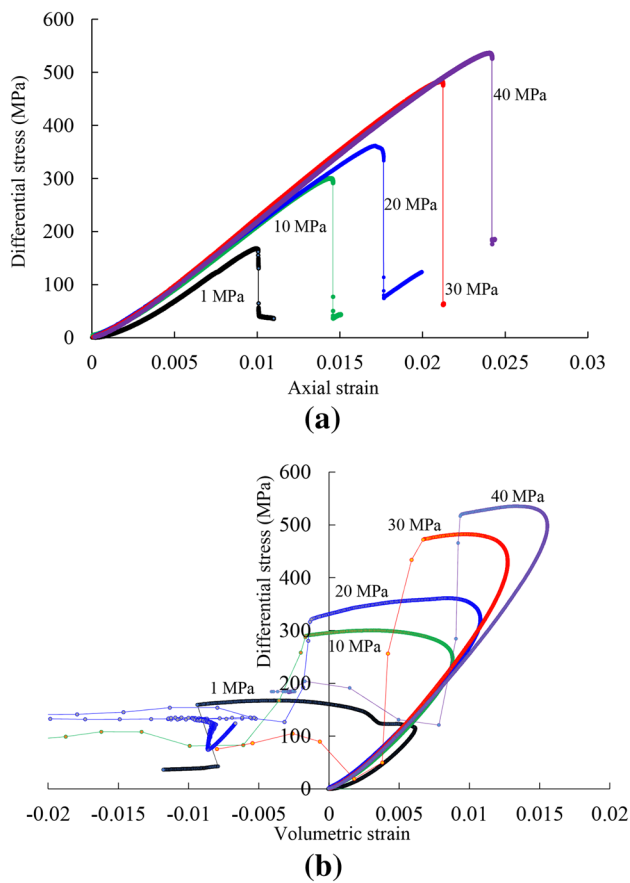


Fig. 3 **a** Stress–axial strain curves and **b** stress–volumetric strain curves of granite under different confining pressures loaded by the axial strain-control

strength, i.e., the class II behavior is observed. The loading is stopped when the differential stress starts to decrease for the specimen under 1 MPa confining pressure, which makes the post-peak stress curve incomplete. The differential stress decreases in a very slow and stable manner for all the specimens, and almost no audible sound is heard during the entire loading and failure process.

Figures 3b and 4b show the differential stress–volumetric strain curves of granite under the two-load control modes, which appear slightly different before the inflection points. The volumetric strain curves obtained by axial strain-control mode (Fig. 3b) appear jagged in the post-peak stage due to the sudden stress drops. In contrast, those obtained under the circumferential strain-control mode are smoother and are associated with more dilation (Fig. 4b).

3.3 Strength Characteristics

In this section, the quantitative mechanical parameters including compressive strength, elastic modulus and crack damage stress are first calculated from the SSCs, which are

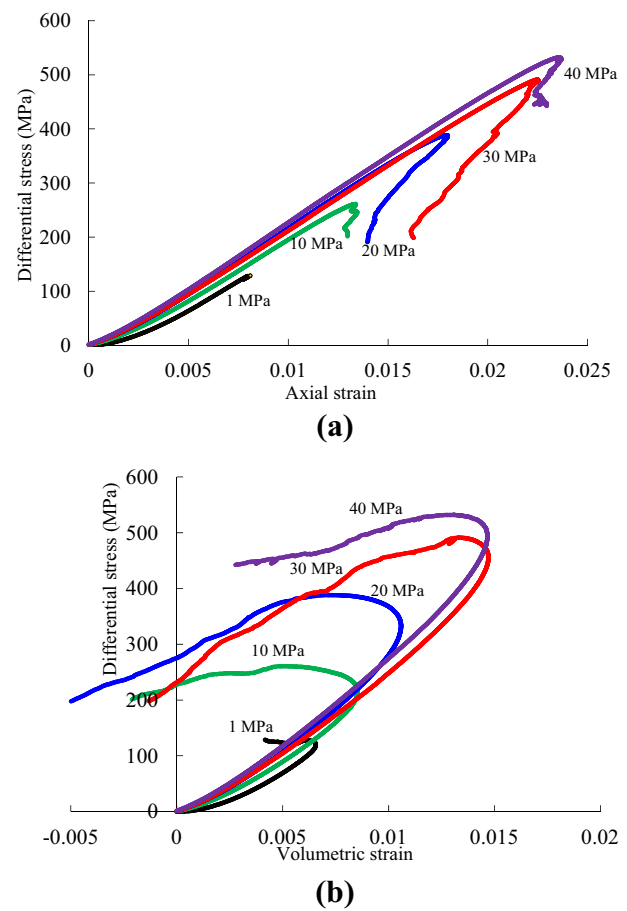


Fig. 4 **a** Stress–axial strain curves and **b** stress–volumetric strain curves of granite under different confining pressures loaded by the circumferential strain-control

then studied and compared with respect to the influences of load control modes on the strength parameters of granite. The elastic modulus is calculated by the slope of the linear portion of SSC in pre-peak stage. The crack damage stress is obtained at the point of volumetric strain curve reversal, corresponding to the commencement of dilation, indicating the onset of unstable crack growth (Bieniawski 1967; Martin and Chandler 1994). The calculated strength data are summarized in Table 1 and plotted in Fig. 5a, b.

Figure 5a is a summary plot of the peak strength and residual strength of granite at different confining pressures under the two-load control modes, which suggests that the peak strength is higher for the axial strain-control than circumferential strain-control when the confining pressure is 1, 10 and 40 MPa. However, the residual strength is much higher for the specimens loaded by the circumferential strain-control mode than the axial strain-control mode. Figure 5b shows the variation of the elastic modulus and crack damage stress with confining pressure. The elastic modulus is generally larger when loaded by axial

Table 1 Strength parameters and fracture angle of granite under different confining pressures loaded by the two control modes

Rock type	Confining pressure (MPa)	Peak strength (MPa)		Residual strength (MPa)		Crack damage stress (MPa)		Elastic modulus (GPa)		Fracture angle (°)	
		Axial	Circum	Axial	Circum	Axial	Circum	Axial	Circum	Axial	Circum
Granite	1	167.4	128.9	39.5	–	114.2	120.1	21.4	21.1	0	0
	10	300.2	261.2	40.3	201.2	247.4	217	23.9	22.8	14	10.5
	20	361.4	388.7	78.4	322	321.5	333.1	22.9	23.9	17	13
	30	482.4	491.5	63.6	198.6	429.5	454.9	25.3	23.9	20	15.5
	40	535.3	532.6	176.7	442.9	499.4	494	25	24	22	20

The “axial” and “circum” in the second row indicate axial strain control and circumferential strain control, respectively

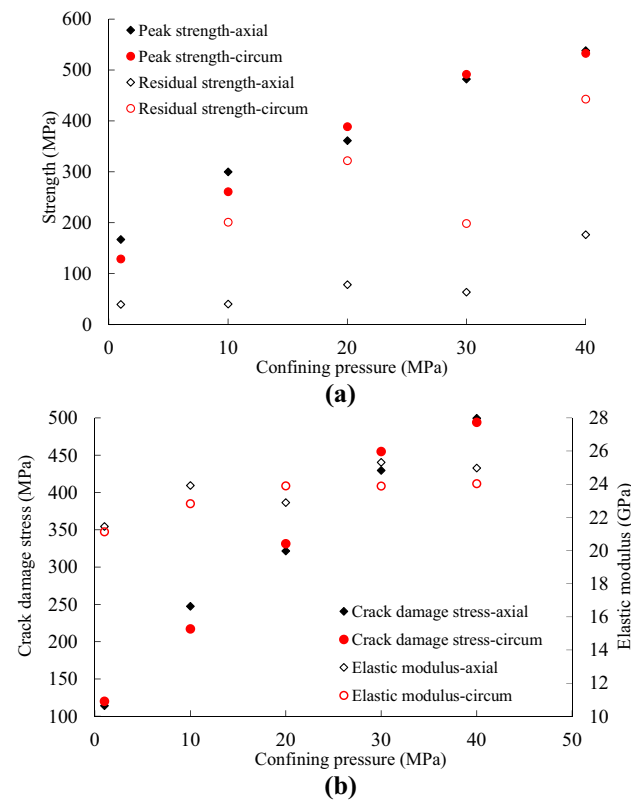


Fig. 5 **a** Peak strength and residual strength, **b** crack damage stress and elastic modulus of granite loaded by the two modes at different confining pressures (“axial” and “circum” indicate axial strain-control and circumferential strain-control, respectively)

strain-control mode. Table 1 shows that the maximum difference of elastic modulus obtained by the two-load control modes is 1.4 GPa. The crack damage stress is found to increase with confining pressure regardless of the load control mode. In contrast, the influence of the load control mode on crack damage stress is insignificant. However, due to the very subtle change of the volumetric strain value around the inflection point, while the differential stress continues to increase, a very accurate determination of the crack damage stress is difficult.

3.4 Failure Modes

Figure 6 shows the photographs of the granite specimens after failure, which exhibit complicated failure modes (rubber bands restrain the rock fragments from falling apart after tests). Under axial strain-control mode, violent failure occurs in granite under 1 MPa confining pressure, and a number of vertical tensile fractures are found to have developed on the surface of the specimen, as indicated by the blue lines on the rock specimen. The number of cracks becomes less for the granite loaded at 10 MPa confining pressure, and both tensile failure and shear fracture are observed. The front surface shows a nearly vertical tensile crack, while two “V” shaped shear cracks (as indicated by the red lines) are found on the back of the surface, as shown in the inset. However, shear failure dominates when the pressure increases to 20 MPa. A traversing shear fracture can be observed on the rock specimen when the confining pressure is 20, 30 and 40 MPa. The failure patterns of granite change from tensile to a mixed form of tensile–shear, and finally to shear failure with increasing confining pressure.

In the circumferential strain-control test, the shear plane in granite is not fully developed (Fig. 6). The rubber band is even not needed to hold the specimens. Only one short vertical fine crack can be observed on the specimen surface under 1 MPa confining pressure (Fig. 6). Slip traces of the fault are also not pronounced as compared with those in the axial control test. The comparison of the fragmented specimens under 20, 30 and 40 MPa pressures reveals that the shear band is wider and more crushed in the axial strain-control test than those in the circumferential strain-control test because of the abrupt rupturing process. These analyses indicate that the failure process is much slower and more stable, and the failure plane is even not fully developed in the circumferential strain-control test.

The fracture angles (the angle between the fracture trace and vertical axis) of granite at different confining pressures under the two-load control modes are calculated (Table 1) and plotted (Fig. 7). For those specimens containing two shear fractures, such as the “V” shaped fracture, the reported

Fig. 6 Photographs of granite specimens after failure (the blue lines on the specimen indicate tensile fractures, while the red lines indicate shear fractures) (colour figure online)

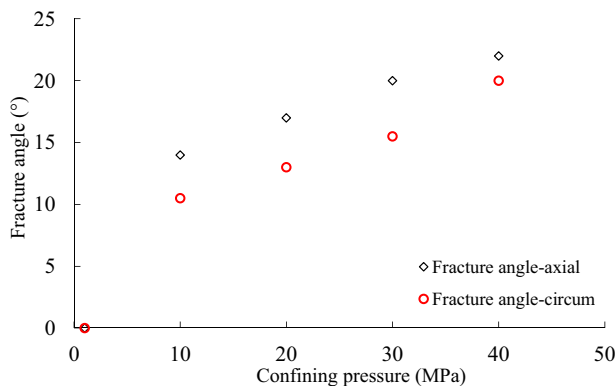
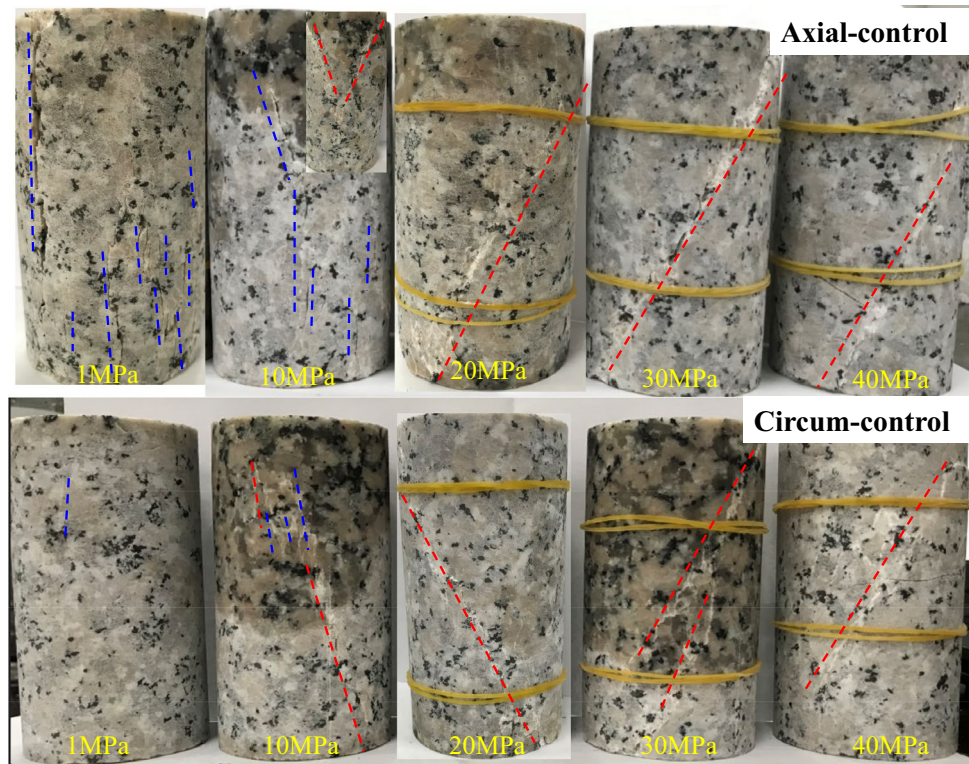


Fig. 7 Fracture angle of granite at different confining pressures under the two-load control modes

fracture angle is determined by the average of the two fracture angles. The results indicate that the fracture angle tends to increase with confining pressure, and the fracture angle is greater in the axial strain-control test than in the circumferential strain-control test under the same confining pressure.

3.5 Acoustic Emissions

The acoustic emission hit rate and energy rate of granite under 40 MPa confining pressure in the axial strain and circumferential strain-control tests are, respectively, shown in Figs. 8 and 9. The hit rate increases gradually with time

(especially after 1000 s) in the axial strain-control test (Fig. 8a). Meanwhile, the energy rate starts to increase rapidly from 2300 s onward, shortly before the sudden rupture, and then peaks at the points of the violent stress drop (Fig. 8b). On the other hand, in the circumferential strain-control test, the AE hit rate is more active than in the axial strain-control test, particularly after changing the load control mode (Fig. 9a). The total number of AE hits are 9.7×10^4 to 12×10^4 , which is much more than in the axial strain-control test (3.2×10^4 to 3.7×10^4 , the range indicates the minimum and maximum accumulative hit number recorded by the four sensors). The peak energy rate in the circumferential strain-control test is not obtained at the point of peak strength but during the differential stress decrease (Fig. 9b), which is one magnitude lower than that in the axial strain test. This indicates that the faulting nucleation and propagation process in the two-load control modes test are different. The faulting process in the axial strain-control test occurs instantaneously, which releases a great amount of elastic energy. In contrast, the faulting process and energy release are progressive in the circumferential strain-control test, and the energy peak can be obtained in a relatively large fracture event.

The above analysis indicates that the energy release at the points of failure is more violent in the axial strain-control test, while the AE hit number, which is often used to evaluate the damage inside the rock, is more in the circumferential strain-control test.

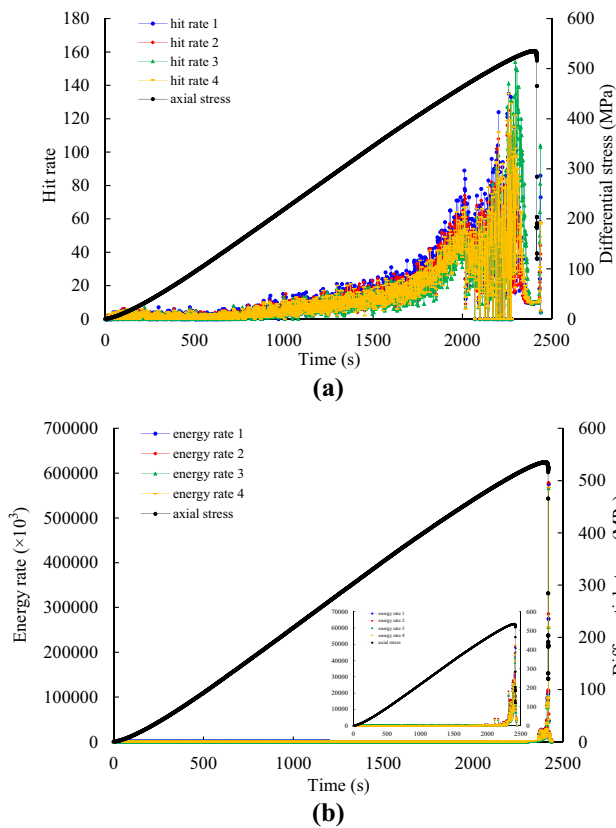


Fig. 8 Variation of AE **a** hit rate and **b** energy rate for granite under 40 MPa confining pressure in axial strain-control test (the small inset in **b** is to better show the increasing trend by deleting several peak values)

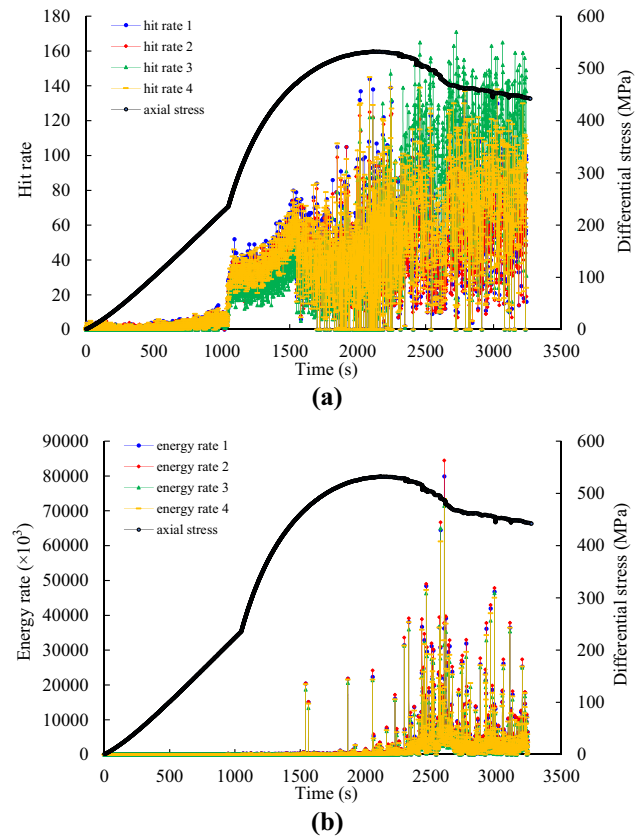


Fig. 9 Variation of AE **a** hit rate and **b** energy rate for granite under 40 MPa confining pressure in circumferential strain-control test (the inflection at about 1000 s is due to the change of loading mode)

4 Mechanism Analysis

4.1 Occurrence Mechanism of Class II SSC

To better understand how class II SSCs are generated, the variation of differential stress, axial and circumferential strain, and stress rate and strain rate with time for granite under 40 MPa confining pressure under the two-load control modes are shown in Figs. 10 and 11. Figure 10a shows that the axial strain is much larger than the circumferential strain. The increase rate of the differential stress first increases and then remains almost constant from 500 to 1500 s, and then gradually decreases (Fig. 10b). The rate of axial strain remains constant as applied in the test ($0.001 \text{ m m/s}/100 \text{ mm} = 0.00001 \text{ s}^{-1} = 10^{-5} \text{ s}^{-1}$), while the rising rate of the circumferential strain increases gradually with time (increase from 10^{-7} to 10^{-5} s^{-1}) before 2200 s, after which it drastically increases as the differential stress approaches the peak stress.

Both the stress, strain and their changing rate show different characteristics for granite when loaded in circumferential strain-control under the same pressure (Fig. 11a, b).

Four distinguishable stages can be divided in the time–differential stress curves (as separated by the three solid lines in Fig. 11a). The first inflection in the curves is due to the change of load control mode, after which the differential stress and strain increase nonlinearly (convex upwards) with time. After the peak stress is reached, the differential stress and strain decrease nonlinearly simultaneously, indicating that no work is done to the rock specimen in this stage because the direction of the axial force and displacement is opposite (i.e., rebound occurs in the specimen). On the contrary, the rock specimen is doing work to the upper loading system. In the last stage, the axial strain starts to increase again, even though the differential stress continues to decrease. This phenomenon suggests that additional work should have been done by the loading system to the rock specimen to maintain the fracture process. The reason that the differential stress continues to decrease, rather than increases like the axial strain is that the bearing capacity of the specimen has been deteriorated after peak strength due to the development of micro-cracks and the shear band.

The stress and strain rates in Fig. 11b increase abruptly when the load control mode is changed. The

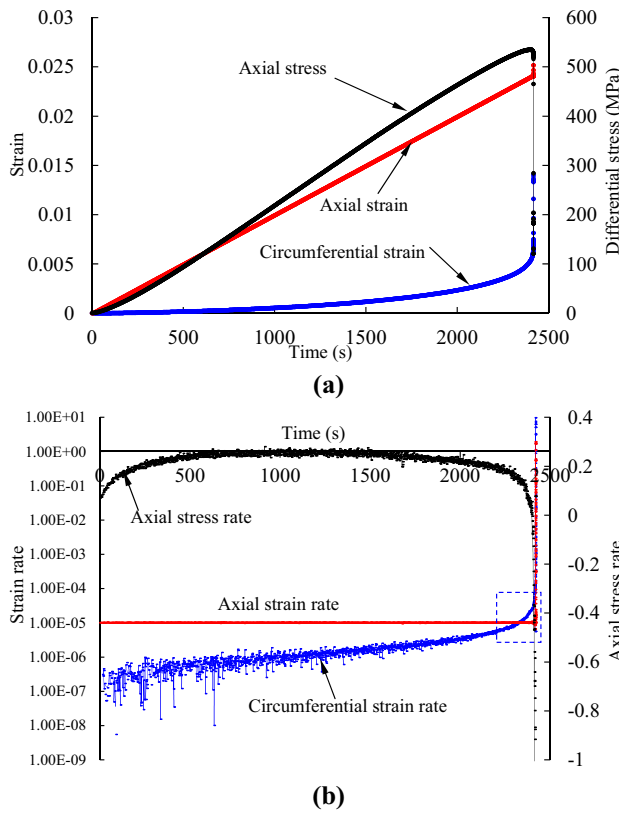


Fig. 10 Variation of **a** axial stress, axial and circumferential strain and **b** axial stress rate, axial and circumferential strain rate with time for granite under 40 MPa confining pressure in axial strain-control test

circumferential strain rate becomes constant ($4.2 \times 10^{-6} \text{ s}^{-1}$) but higher than that before the change. The differential stress rate and axial strain rates gradually decrease to values which are much lower than those before the change. The comparison of the strain rate in Figs. 10b and 11b indicates that the circumferential strain rate is much smaller in the circumferential strain-control test than in the axial strain-control test as the stress approaches the peak strength ($4.2 \times 10^{-6} \text{ s}^{-1}$ versus 10^{-5} – 10^{-4} s^{-1}). After the crack damage stress is reached during the compression of rock specimen in the axial strain-control test, the cracks develop and propagate rapidly in the specimen (Martin and Chandler 1994), which leads to the fast and large dilation. In the circumferential strain-control test, the circumferential strain rate is set to be a constant and small value, which makes the dilation (i.e., the propagation and coalescence of cracks) slow, controllable and stable. That is why the class II SSCs develop slowly and stably in the compression test, even for the hard brittle granite. On the other hand, both the circumferential strain and strain rate increase dramatically before the peak strength is reached in the axial strain-control test, which means that

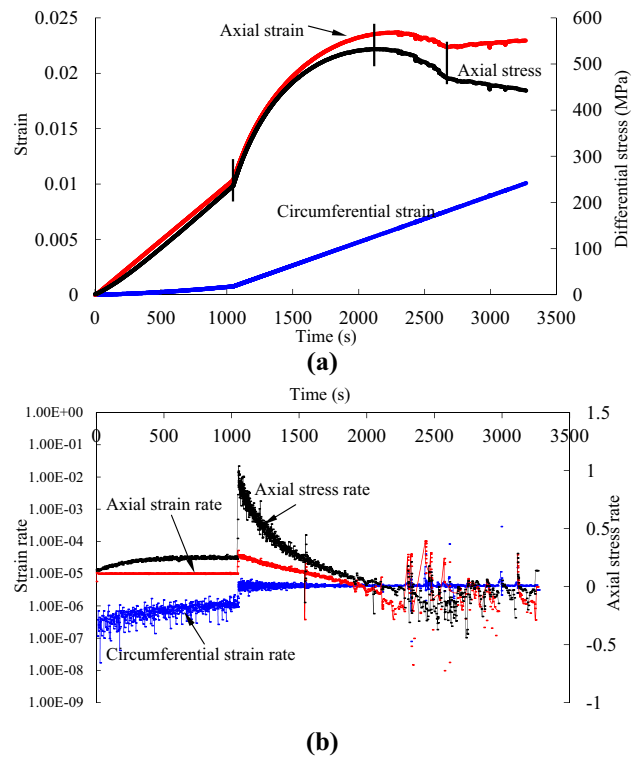


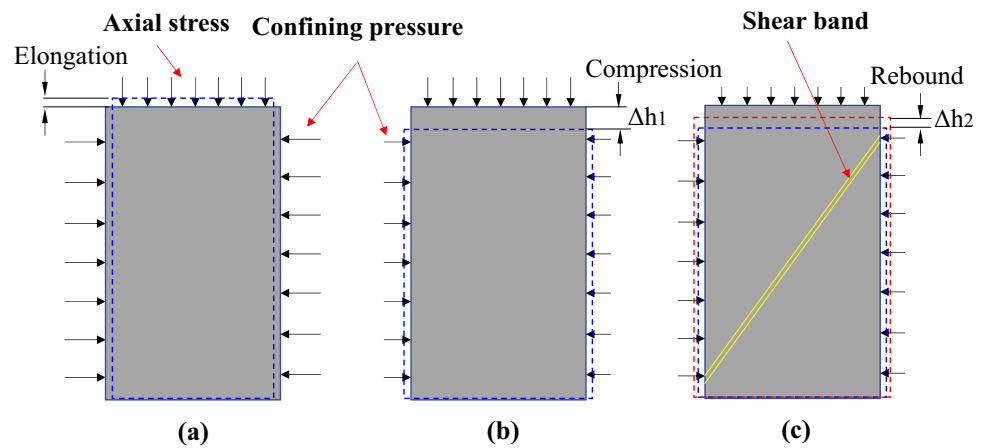
Fig. 11 Variation of **a** axial stress, axial and circumferential strain and **b** axial stress rate, axial and circumferential strain rate with time for granite under 40 MPa confining pressure in circumferential strain-control test

the failure process of the rock specimen is instantaneous and uncontrollable.

The above analyses indicate that the load control mode has a significant influence on the stress and strain characteristics as well as the stress and strain rate for the test granite. Both the axial strain rate and circumferential strain rate are smaller in the circumferential strain-control test than in the axial strain-control test as the stress approaches the peak strength. In the axial strain-control test, the cracks grow and propagate fast when the stress is above the crack damage stress (Martin and Chandler 1994), and the crack propagation is unstable, leading to the drastic dilation. The crack growth in the specimens becomes controllable and stable when the axial load is applied in a circumferential strain-control test at a very low rate.

The positive post-peak modulus of class II SSC is due to the decrease of axial strain after the peak strength (the rock specimen is shortened and axial strain increases in the pre-peak stage, while the specimen elongates and the strain decreases in the post-peak stage), which is attributed to the following two possible reasons. The first is the action of the very high confining pressure. The length in the axial direction will be extended due to the Poisson effect, as shown in Fig. 12a. The second reason is due to the unloading of

Fig. 12 Schematic diagram of the loading and deformation in the triaxial test. The black solid line, the blue dotted line and the red dotted line represent the original specimen shape, the shape before peak strength and the shape after peak strength, respectively. **a** When the confining pressure is larger than the axial stress, **b** when the confining pressure is smaller than the axial stress and before peak strength, **c** shear band develops in the post-peak stage, and rebound occurs (colour figure online)



the differential stress. Part of the deformation along the axial direction will be recovered during the differential stress decrease, which will elongate the specimen (i.e., the axial strain decreases). Because the circumferential strain increases monotonically in the test (Fig. 11a), and dilation rather than compression occurs in the lateral direction, thus the first reason can be excluded. As such, the decrease of the axial strain in the post-peak stage is related to the unloading in the axial direction. Figure 12b, c schematically shows the change of axial deformation during loading. The rock specimen is compressed when the differential stress gradually increases, and the axial compressive deformation is Δh_1 . The shear band gradually forms after the peak compressive strength is reached due to the crack coalescence along the direction of the maximum shear stress. The compressive deformation within the shear band is irreversible because of the fracture and cataclastic failure of rock. On the other hand, the other parts of rock below and above the shear band have not been completely damaged, although some discrete cracks have also initiated and propagated in them. The compressive deformation within these portions of rocks is composed of reversible elastic deformation and irreversible deformation, the former of which will be recovered when the differential stress decreases after the peak strength (Δh_2 in Fig. 12c).

The above analyses show how the class II SSC with positive post-peak modulus is generated, and why the associated failure process is slow, stable and controllable. The class II behavior of rock is similar to the stress–strain curve of the pre-peak axial stress unloading test in both form and nature. One difference is that the circumferential strain still increases during the post-peak decrease of axial strain in the class II behavior, indicating that the accumulated energy in the specimen is sufficient to maintain the extension of lateral deformation. During pre-peak unloading, on the other hand, the lateral strain no longer increases once the axial load is removed.

4.2 Influencing Factors of the Class II SSC

The uniaxial compression tests conducted by Vogler and Stacey (2016) have shown that the uniaxial compressive strength, post-peak modulus and fracture angle of anorthosite decrease with increasing height-to-diameter ratio when loaded by circumferential strain-control mode (generating class II SSC, as schematically shown in Fig. 13). The authors also found that the test specimens with height-to-diameter ratios < 1 may exhibit class I behavior even loaded by circumferential strain-control. Based on these findings, they concluded that the class I or class II behavior of rock in laboratory testing is partially a test specimen-dependent phenomenon and not solely an intrinsic characteristic of the rock material.

When the standard cylindrical specimens ($\Phi 50 \times 100$ mm) are tested with the circumferential strain-control (the external conditions such as the test system stiffness, loading mode

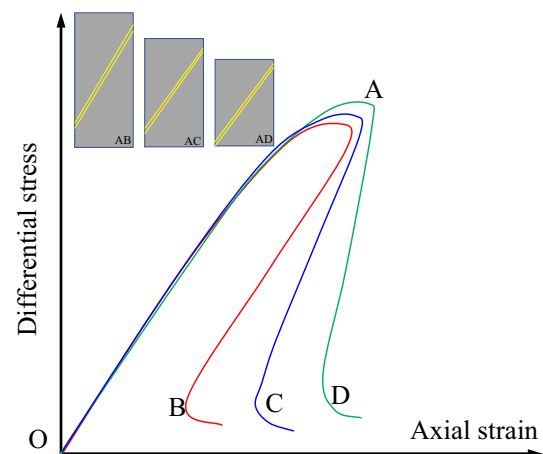


Fig. 13 Schematic diagram of class II stress–strain curves with different rock specimen geometries (modified from Vogler and Stacey (2016))

and loading rate remain constant), the SSCs of different rock types may also show different characteristics. To obtain a better understanding of the deformation behavior of class II curves, and to take advantage of the class II stress curve as a practical means to reflect rock properties, it is important to identify what dictates the post-peak modulus and the terminal point of the stress decrease in the post-peak stage of class II SSC.

Figure 14 schematically shows three typical class II SSC (curves OAB, OAC, OAD). For the granite loaded under confining pressure of 20 and 30 MPa, the extent of stress decrease is larger than others (similar to curves OAB and OAC), while for the less brittle rock such as sandstone, the post-peak slope is much larger than that of the granite (similar to curve OAD).

As discussed in Sect. 4.1, the decrease in axial strain (the positive post-peak modulus) is due to the unloading and rebound of rock during differential stress decrease. The smaller post-peak modulus of curve OAB than that of curve OAD indicates that more elastic deformation is recovered in curve OAB than curve OAD during the stress decrease. For rocks characterized by curve OAB, more elastic energy is released than rocks with curve OAD in the post-peak stage. Considering that the energy accumulation and consumption is similar for the two rocks in the pre-peak stage (because they have similar SSC, Fig. 14), and the test system no longer does work to the specimen after the peak strength, more elastic energy which is stored in the specimen is consumed for curve AD than curve AB either in the form of plastic deformation or initiation and propagation of new cracks, leading to less reversible axial strain.

Curves OAB and OAC (Fig. 14) have similar post-peak modulus but different reversal strain. For curve OAC, the rebound of the axial strain continues until reaching a much

smaller axial strain and stress. However, for curve OAB, the recovery of axial strain stops after a comparatively smaller decrease in differential stress and strain. The reversal of the axial strain at points B and C indicates that the loading system starts to do work to the rock specimen again. For the same rock type, if a higher proportion of elastic energy is stored in the specimen before peak stress, the rebound of axial strain will be more pronounced, which corresponds to curve OAC. In contrast, if a higher proportion of energy is consumed by the plastic deformation before peak strength, the post-peak modulus will be high and the decrease of differential stress and strain will be small. On the other hand, if less energy is consumed in the form of plastic deformation or initiation and propagation of new cracks in the post-peak stage, the extent of decrease in differential stress and axial strain will be large.

The above analysis indicates that the shape of the class II SSC in the post-peak stage (post-peak modulus, the amount of the reversal axial strain and the decrease extent of differential stress) is closely associated with the proportion of elastic energy to dissipated energy in the pre-peak stage and the consumed energy with respect to plastic deformation or initiation and propagation of new cracks in the post-peak stage. The two aspects are dictated by the rock properties if the external conditions such as the test system stiffness, specimen geometry, loading mode and loading rate remain constant.

4.3 Influences of Load Control Modes on Rock Properties

The two-load control modes differ in two fundamental aspects. Firstly, the circumferential strain is used as the feedback signal to control the application of the axial load, which avoids the sudden and drastic increase of lateral deformation when approaching failure. Secondly, the deformation rate is much lower for the circumferential strain-control mode than the axial strain-control mode. Figure 11 indicates that both the axial and circumferential strain rates in the circumferential strain-control test are one magnitude lower than those in the axial strain-control test.

The much lower and constant circumferential deformation rate is regarded as the dominant factor that leads to the different mechanical behavior of granite when loaded under the axial and circumferential strain-control. It is well known that the strain rate has a great impact on the mechanical properties of rock (Sano et al. 1981; Lajtai et al. 1991; Fuenkajorn and Kenkhunthod 2010; Li et al. 2014; Zhang and Zhao 2014), and a number of experimental studies have shown that the uniaxial compressive strength and elastic modulus of rock increase with strain rate (Fuenkajorn and Kenkhunthod 2010; Li et al. 2014), which is consistent with the findings in the present study.

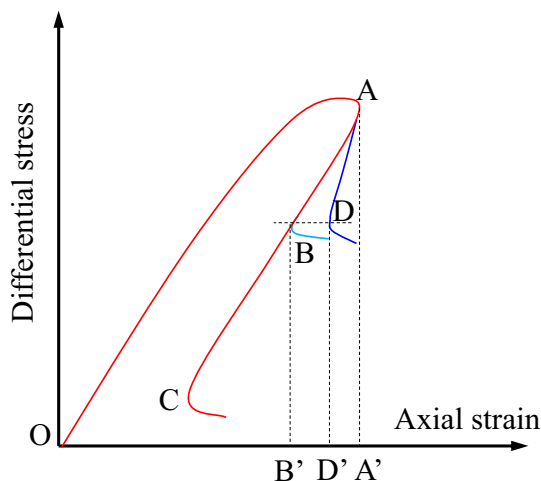


Fig. 14 Schematic diagram of class II stress–strain curves with different post-peak modulus and reversal strain

Based on the Mohr–Coulomb strength criterion, σ_1 and σ_3 should satisfy Eq. (1) or (2) when failure occurs:

$$\sigma_1 = \sigma_3 \frac{1 + \sin \varphi}{1 - \sin \varphi} + 2c \sqrt{\frac{1 + \sin \varphi}{1 - \sin \varphi}}, \quad (1)$$

$$\sigma_1 = \sigma_3 \tan^2 \left(45^\circ + \frac{\varphi}{2} \right) + 2c \cdot \tan \left(45^\circ + \frac{\varphi}{2} \right), \quad (2)$$

where σ_1 and σ_3 are the maximum and minimum principal stress, and c and φ are cohesion and internal friction angle. Based on the geometrical relationship in the Mohr's circle, $2\alpha_f = 90^\circ + \varphi$, and $\alpha_f = 45^\circ + (\varphi/2)$. α_f is the angle between the fracture plane and the direction of σ_3 (note that α_f here and the fracture angle discussed in Sect. 3.4 are complementary). As such, Eq. (2) can be rewritten as:

$$\sigma_1 = \sigma_3 \tan^2 \alpha_f + 2c \cdot \tan \alpha_f. \quad (3)$$

Equation (3) indicates that the compressive strength of rock will increase with the rise of α_f if the cohesion of rock remains constant under a given confining pressure. In the present study, α_f varies in the range of 68° – 80° for granite in the triaxial compression test. The fracture angle of rock specimen is found to be larger in the axial strain-control test than that in the circumferential strain-control test. In other words, α_f is lower in the axial strain-control test. As such, the compressive strength of rock when loaded in axial strain-control will be lower than that under circumferential strain-control based on Eq. (3) if the cohesion c is treated as the same in the two tests under the same confining pressure. This prediction of the compressive strength is not consistent with the measured results because the compressive strength is found to be higher in the axial strain-control test under the same confining pressure. The different degree of cohesion weakening in rocks when loaded by the two control methods is considered to lead to the higher compressive strength but lower α_f in the axial strain-control test.

Based on the study of Martin and Chandler (1994), the cohesion of rock gradually deteriorates in the loading process, and the cohesion does not contribute much to the compressive strength of rock once the fracture plane is generated and the sliding of rock fracture occurs, after which friction strength is fully mobilized. In the circumferential strain-control test, the deformation rate is lower than that in the axial strain-control test, and higher AE hit rates are generated during loading (as presented in Sect. 3.5), indicating that more cracks and damage have occurred in the rock specimens. The generated micro-cracks lead to a larger extent of cohesion weakening in rocks. On the other hand, the micro-cracks are less developed in the axial strain-control test before the final rupture because of the higher deformation rate, which can be inferred from the fewer acoustic emission hits in Sect. 3.5. As such, the degradation of cohesion is less pronounced

before the peak strength. Therefore, in Eq. (3), a larger α_f but a much smaller c can result in a lower compressive strength of rock in the circumferential strain-control test.

5 Discussion

The circumferential strain-control method has been used in the uniaxial and triaxial compression test for decades to obtain the complete SSC of brittle rocks (class II curves). The complete SSC (especially in the post-peak stage) can be obtained even for brittle granite by adopting a low constant circumferential strain rate. Besides, the elastic energy accumulates in the specimens before the peak strength can be released by itself in the post-peak stage because of the unrestricted axial strain, which will lead to the decrease (partial recovery) of the axial strain.

Compared with the axial strain-control test under the same confining pressure, the cracking occurs in a much slower and more stable manner in the circumferential strain-control test, while the damage is more developed inside the specimen which can be inferred from the number of AE hit rate. In the axial strain-control test, the crack coalescence occurs rapidly once the peak strength is reached, and the shear band then forms which is accompanied by a large post-peak stress drop.

The investigation of the class II SSCs of different rocks is of great significance for the evaluation of dynamic geohazard such as rockburst in deep tunnel and mining. The occurrence of a rockburst is closely related to the energy accumulation and release of the surrounding rock under loading (Gong et al. 2019a, b; Meng et al. 2019; Yan et al. 2019). Based on the analysis in Sect. 4.2, the shape of class II SSC in the post-peak stage is associated with the inherent property of rock when the testing system, specimen geometry and test method are comparable. Before peak strength, elastic energy accumulates in the specimen due to the work done by the test system. Meanwhile, part of the work is consumed by the plastic deformation, crack initiation and growth before peak strength. In the post-peak stage, only the stored elastic energy before the peak strength will be used to fracture the rock specimen because no additional work is done by the test system. On the contrary, the specimen will do work to the test system, i.e., some stored elastic energy will be released. If more elastic energy builds up in the specimen before the peak strength, and less energy is consumed in the post-peak stage, the post-peak modulus will be smaller, and the reversal strain will be larger. As such, the shape of the class II SSC is associated with the manner of the elastic energy accumulation and dissipation (with respect to plastic deformation and crack initiation and propagation) in the pre-peak stage, and the energy release and consumption (with respect to crack coalescence and formation of shear band) in

the post-peak stage. If a higher proportion of elastic energy is accumulated in the specimen before the peak strength and less energy is consumed in the post-peak stage (with smaller post-peak modulus and larger reversal axial strain), the failure process of brittle rock in the in situ rock engineering will be violent due to the great amount of elastic energy release. As such, the class II SSC can be used to evaluate the rockburst proneness of a particular rock, which is dictated by the energy accumulation and release.

Axial strain or load control method is often used in the compression test to obtain the class I SSC because of the simpler test procedure and more intuitive test results. The post-peak behavior of the class I SSC is often used to qualitatively evaluate the potential of strain rockburst. If the peak strength drops to a low value and rock fragment ejection occurs in the laboratory compression test, rockburst is also likely to occur during the excavation of deep tunnel. Quantitative indices have been developed based on the class I SSC to assess the possibility of rockburst (Meng et al. 2015). For those very hard and brittle rocks such as marble, granite, basalt and quartzite, the peak strength drops drastically to a low value or even to zero when failure occurs. The shape of the post-peak SSC is similar, which makes the quantitative assessment and further differentiation of rockburst proneness difficult for different rocks. On the other hand, different rock types are characterized by different class II stress–strain behavior with respect to the post-peak modulus, amount of reversal strain and magnitude of differential stress decrease. As such, the rockburst proneness can be differentiated, quantitatively assessed and compared among different rock types.

Class I and class II SSCs can be used together to evaluate the potential of strain rockburst in deep tunnel and mining. Specimen geometry and loading rate should be standardized to obtain the class II SSC of rock for a comparison of the post-peak behavior. More triaxial tests on different rock types need to be conducted to obtain the class II SSCs, and to quantitatively compare and evaluate the rockburst potential under the same stress state.

The present study shows that the load control modes (axial strain-control or circumferential strain-control) have great influences on the mechanical behavior (compressive strength, elastic modulus, failure modes and fracture angle) of rocks. Therefore, caution should be taken when interpreting the mechanical parameters obtained in the compression test loaded by different control methods.

6 Conclusions

Triaxial compression tests are conducted on granite, and the influences of load control mode (i.e., axial strain-control and circumferential strain-control) on the compressive

strength, elastic modulus, failure modes and acoustic emission characteristics are studied and compared. The occurrence mechanism and influencing factors of class II SSC are investigated, and the potential application of the class II SSC in the evaluation of brittle failure of hard rock is also discussed. The main conclusions drawn from this study are summarized as follows:

1. The final rupture is violent for granite (in the form of rapid stress drop after peak strength) in the axial strain-control test, while the failure process is very slow and stable in the circumferential strain-control, which is due to the much lower and constant lateral deformation rate.
2. The peak strength, elastic modulus and fracture angle are found to be higher in the axial strain-control test than in the circumferential strain-control test under the same confining pressure. The first two larger strength parameters are due to the higher loading rate in the axial strain-control test, while the larger fracture angle is associated with more damage and cohesion weakening inside the rock, which can be inferred from the more AE hits in circumferential strain-control test.
3. The occurrence of class II SSC is attributed to the elastic axial strain rebound during the release of the stored elastic energy in the post-peak stage. The shape of class II SSC is dependent on the proportion of elastic energy to dissipated energy in the pre-peak stage, and the consumed energy with respect to plastic deformation or initiation and propagation of new cracks in the post-peak stage. The above are dictated by the rock property if the loading condition and specimen geometry remain constant.
4. The class II SSC of rock specimens obtained in the laboratory can aid the differentiation of the energy accumulation and consumption of different hard and brittle rocks, which are usually characterized by a more abrupt and larger stress drop in the axial strain-control test. The strain rockburst potential of a particular rock type can be thus effectively evaluated.

Acknowledgements We gratefully acknowledge the financial support from the Open Fund (PLN201703) of the State Key Laboratory of Oil and Gas Reservoir Geology and Exploitation (Southwest Petroleum University), the National Natural Science Foundation of China under Grant nos. 51609121, 51879135, 41877217. The work in this paper was also supported by the Natural Science Foundation of Shandong Province (Grant no. ZR2016EEQ 22), and the Hong Kong Scholars Program (XJ2017043). The first author acknowledges the support from the General Research Fund 2017/18 (#17303917) of the Research Grants Council of the University Grants Committee, Hong Kong, and the Hung Hing Ying Physical Sciences Research Fund 2017–18. The third author acknowledges the support from the Postgraduate Scholarship from the University of Hong Kong, and the Pilot Scheme on International Experience of RPg students 2016–2017.

Compliance with Ethical Standards

Conflict of interest The authors declare that they have no conflict of interest.

References

- Ai C, Zhang J, Li YW, Zeng J, Yang XL, Wang JG (2016) Estimation criteria for rock brittleness based on energy analysis during the rupturing process. *Rock Mech Rock Eng* 49(12):4681–4698
- Bieniawski ZT (1967) Mechanism of brittle fracture of rock, parts I, II and III. *Int J Rock Mech Min Sci Geomech Abstr* 4:395–430
- Bieniawski ZT, Bernede MJ (1979) Suggested methods for determining the uniaxial compressive strength and deformability of rock materials. *Int J Rock Mech Min* 16(2):137–140
- Cai P, Wu AQ, Wang B, Zheng BH (2010) A rockburst proneness index based on class II whole process curve. *Chin J Rock Mech Eng* 29(S1):290–294
- Chen SJ, Guo WJ, Liu JX, Yin LM (2010) Experiment on formation mechanism of rock class II curve. *J China Coal Soc* 35(S):54–58
- Chen L, Wang CP, Liu JF, Liu J, Wang J, Jia Y, Shao JF (2015) Damage and plastic deformation modeling of Beishan granite under compressive stress conditions. *Rock Mech Rock Eng* 48(4):1623–1633
- Fairhurst C, Hudson J (1999) Draft ISRM suggested method for the complete stress–strain curve for intact rock in uniaxial compression. *Int J Rock Mech Min Sci* 36:279–289
- Fuenkajorn K, Kenkhunthod N (2010) Influence of loading rate on deformability and compressive strength of three Thai sandstones. *Geotech Geol Eng* 28:707–715
- Gong F, Yan J, Li X, Luo S (2019a) A peak-strength strain energy storage index for rock burst proneness of rock materials. *Int J Rock Mech Min Sci* 117:76–89
- Gong F, Yan J, Luo S, Li X (2019b) Investigation on the linear energy storage and dissipation laws of rock materials under uniaxial compression. *Rock Mech Rock Eng*. <https://doi.org/10.1007/s00603-019-01842-4>
- Kovari K, Tisa A, Einstein HH, Franklin JA (1983) Suggested methods for determining the strength of rock materials in triaxial compression. *Int J Rock Mech Min Sci Geomech Abstr* 20(6):285–290
- Labuz JF, Biolzi L (1991) Class I vs class II stability: a demonstration of size effect. *Int J Rock Mech Min Sci Geomech Abstr* 28(2–3):199–205
- Lajtai EZ, Scott Duncan EJ, Carter BJ (1991) The effect of strain rate on rock strength. *Rock Mech Rock Eng* 24:99–109
- Li Y, Huang D, Li X (2014) Strain rate dependency of coarse crystal marble under uniaxial compression: strength, deformation and strain energy. *Rock Mech Rock Eng* 47(4):1153–1164
- Lockner D (1993) The role of acoustic emission in the study of rock fracture. *Int J Rock Mech Min Sci Geomech Abstr* 30(7):883–899
- Lockner DA, Byerlee JD, Kuksenko V, Ponomarev A, Sidorin A (1991) Quasi-static fault growth and shear fracture energy in granite. *Nature* 350:39–42
- Martin CD, Chandler NA (1994) The progressive fracture of Lac du Bonnet granite. *Int J Rock Mech Min Sci Geomech Abstr* 31(6):643–659
- Meng FZ, Zhou H, Zhang C, Xu R, Lu J (2015) Evaluation methodology of brittleness of rock based on post-peak stress–strain curves. *Rock Mech Rock Eng* 48(5):1787–1805
- Meng FZ, Wong LNY, Zhou H, Yu J, Cheng GT (2019) Shear rate effects on the post-peak shear behaviour and acoustic emission characteristics of artificially split granite joints. *Rock Mech Rock Eng* 52(7):2155–2174
- Munoz H, Taheri A, Chanda EK (2016a) Fracture energy-based brittleness index development and brittleness quantification by pre-peak strength parameters in rock uniaxial compression. *Rock Mech Rock Eng* 49(12):4587–4606
- Munoz H, Taheri A, Chanda EK (2016b) Pre-peak and post-peak rock strain characteristics during uniaxial compression by 3D digital image correlation. *Rock Mech Rock Eng* 49(7):2541–2554
- Nishiyama T, Chen Y, Kusuda H, Ito T, Kaneko K, Kita H, Sato T (2002) The examination of fracturing process subjected to triaxial compression test in Inada granite. *Eng Geol* 66(3–4):257–269
- Okubo S, Nishimatsu Y (1985) Uniaxial compression testing using a linear combination of stress and strain as the control variable. *Int J Rock Mech Min Sci Geomech Abstr* 22:323–330
- Okubo S, Nishimatsu Y, He C (1990) Loading rate dependence of class II rock behaviour in uniaxial and triaxial compression tests—an application of a proposed new control method. *Int J Rock Mech Min Sci Geomech Abstr* 27(6):559–562
- Sano O, Ito I, Terada M (1981) Influence of strain rate on dilatancy and strength of Oshima granite under uniaxial compression. *J Geophys Res Solid Earth* 86(B10):9299–9311
- Sano O, Terada M, Ehara S (1982) A study on the time-dependent microfracturing and strength of Oshima granite. *Tectonophysics* 84:343–362
- Tapponnier P, Brace WF (1976) Development of stress-induced microcracks in Westerly granite. *Int J Rock Mech Min Sci Geomech Abstr* 13(4):103–112
- Tarasov BG, Potvin Y (2013) Universal criteria for rock brittleness estimation under triaxial compression. *Int J Rock Mech Min Sci* 59:57–69
- Vogler U, Stacey TR (2016) The influence of test specimen geometry on the laboratory-determined Class II characteristics of rocks. *J S Afr Inst Min Metall* 116(11):987–1000
- Wang CS, Zhou HW, Wang ZH, Pei H, Liu JF (2017) Investigation on the rockburst proneness of beishan granite under different stress state. *Adv Eng Sci* 49(6):84–90
- Wawersik WR, Fairhurst C (1970) A study of brittle rock fracture in laboratory compression experiments. *Int J Rock Mech Min Sci Geomech Abstr* 7(5):561–575
- Wong TF (1982) Micromechanics of faulting in Westerly granite. *Int J Rock Mech Min Sci Geomech Abstr* 19(2):49–64
- Yan C, Jiao YY, Yang S (2019) A 2D coupled hydro-thermal model for the combined finite-discrete element method. *Acta Geotech* 14(2):403–416
- Zhang QB, Zhao J (2014) A review of dynamic experimental techniques and mechanical behaviour of rock materials. *Rock Mech Rock Eng* 47(4):1411–1478
- Zheng Y, Chen C, Liu T, Zhang H, Xia K, Liu F (2018) Study on the mechanisms of flexural toppling failure in anti-inclined rock slopes using numerical and limit equilibrium models. *Eng Geol* 237:116–128

Publisher's Note Springer Nature remains neutral with regard to jurisdictional claims in published maps and institutional affiliations.